ACI STRUCTURAL JOURNAL TECHNICAL PAPER

Title No. 118-S23

Basalt Fiber-Reinforced Polymer-Confined Geopolymer Concrete

by Junaid Ahmad, Tao Yu, and Muhammad N. S. Hadi

This paper investigates the behavior of basalt fiber-reinforced polymer (BFRP) confinement on geopolymer concrete (GPC) cylinders under axial monotonic compression. Results were compared with glass fiber-reinforced polymer (GFRP) confinement on GPC cylinders. Effects of confinement on failure mode, stress-strain behavior, peak axial compressive stress, and ultimate axial strain of the tested specimens were ascertained and discussed. It was observed that the confinement of BFRP is more effective than the GFRP due to the higher elastic modulus and larger rupture strain of the former. Results were also compared with the existing stress-strain models for FRP confined ordinary portland cement concrete (OPC). It was observed that the existing stress-strain models generally cannot provide accurate predictions of the stress-strain behavior of FRP confined GPC. It was concluded that BFRP confined GPC can be considered as a sustainable alternative to the FRP confined OPC.

Keywords: basalt; basalt fiber-reinforced polymer (BFRP); compressive behavior; confined geopolymer concrete; geopolymer concrete; glass fiber-reinforced polymer (GFRP); stress-strain model.

INTRODUCTION

Geopolymer concrete (GPC) is being promoted worldwide to reduce the carbon footprints of the construction industry.[1,2] As it is well known, cement is a main constituent and binder used in normal concrete. Its production results in carbon dioxide emissions of almost the same quantity as that of cement produced.[3] Geopolymer concrete is considered to be a green concrete, which is a sustainable and environmentally friendly replacement of normal concrete.[4] GPC not only reduces the carbon related emissions but also uses industrial wastes such as fly ash and ground-granulated blast-furnace slag.[5]

Geopolymer concrete is observed to be more brittle as compared to ordinary portland cement concrete (OPC).[3,6] Pan et al.[7] also observed that the GPC showed a lower fracture energy and lower ductility than the OPC. Noushini et al.[8] observed that the curing condition of the GPC affects the brittleness of the GPC. They observed that the heat-cured GPC showed higher strength and lower axial strains at peak stress than the ambient-cured GPC. Also, the GPC specimens cured in sealed ambient conditions resulted in a higher axial strain at peak stress than the heat-cured ones. This observation was in contradiction to the general understanding that GPC resulted in lower axial strain at peak stress than the OPC. One of the main reasons of this general understanding is that most of the research work directed in the field of GPC was targeted on heat-cured GPC.

Fiber-reinforced polymer (FRP)-confined GPC columns provide an attractive alternative to FRP-confined OPC. The FRP confinement is a source of strength and ductility enhancement.[9,10] A sustainable natural fiber-based FRP confinement of the GPC will lead to the development of a complete sustainable replacement to the FRP-confined OPC. Basalt fiber is a natural fiber that is produced by using basalt rocks with the help of a melting process without any addition of further additives.[11] Basalt fibers are considered to be with high strength, high resistance to fire, high chemical resistance, and high impact resistance as compared to E-glass fibers.[12] Basalt fiber-reinforced polymer (BFRP) is considered a sustainable and environmentally friendly natural FRP.[13] Therefore, BFRP-confined GPC can be considered as a sustainable replacement to the conventionally used FRP (such as glass FRP or GFRP)-confined OPC.

Lokuge and Karunasena[14] studied the ductility behavior of FRP-confined GPC. The study concluded that the stress-strain behavior of FRP-confined GPC is different from the FRP confined OPC. Ozbakkaloglu and Xie[15] is the only study on the GPC-filled FRP tubes (GPCFFT). They investigated the axial stress-strain behavior of GPCFFT and the results were compared with the OPC-filled FRP tubes (OPCFFT). The compressive strength of the unconfined GPC and OPC used in the study was in the range of 20 to 25 MPa (2900 to 3625 psi). It was observed that the increase of strain at peak stress due to GFRP, carbon FRP (CFRP), and BFRP confinement was less in the GPCFFT than in OPCFFT. The same observation was made for the strength enhancement except for the CFRP-confined specimens. The CFRP confinement behaved differently and strength enhancement with CFRP confinement was more for GPCFFT than the OPCFFT. This observation was attributed to the variation in the experimental test results as the difference in average strength enhancement ratio for CFRP-confined GPC and OPC was very small.

Ozbakkaloglu and Xie[15] modified the previously proposed ultimate condition prediction equations by Ozbakkaloglu and Lim[16] for FRP-confined OPC to be applicable to the GPCFFT. The study did not compare the experimental results with the other existing models for OPC. Also, the modification was proposed on the basis of only one experimental study with relatively low unconfined concrete strengths (that is, 20 to 25 MPa [2900 to 3625 psi]).

In view of the stated background, it can be observed that the behavior of FRP-confined GPC can be different than the FRP-confined OPC. There is a strong need of further

ACI Structural Journal, V. 118, No. 1, January 2021.

MS No. S-2020-075, doi: 10.14359/51728094, received February 27, 2020, and reviewed under Institute publication policies.

experimental studies to fully understand the behavior of BFRP confinement on GPC. Also, the applicability of existing confinement models of FRP-confined OPC for FRP-confined GPC needs further investigation. This study was conducted to ascertain the behavior of FRP-confined GPC under axial compression and the results were compared with the existing confinement models for the FRP-confined OPC. The test parameters adopted were the number of FRP layers and type of the FRP confinement.

RESEARCH SIGNIFICANCE

This study will be helpful in understanding the behavior of a newly proposed compression member, BFRP-confined geopolymer concrete. Also, this study will provide a baseline to the further research in the development of a confinement model for this sustainable compression member. This in turn will address the sustainability challenges in the construction industry.

MATERIALS

Geopolymer concrete (GPC)

Ambient cured GPC with a target strength of 45 MPa (6526 psi) was prepared in the laboratory. Trial tests were conducted to develop the mixture design of the GPC. The GPC mixture design proposed by Hadi et al.[17] was used as the baseline. Further trial tests were conducted to modify the same mixture design for the particular materials used in this study. The GPC mixture proportions adopted in this study are presented in Table 1. The alkali to binder ratio in the proposed mixture design was 0.35 and sodium silicate to sodium hydroxide ratio was 2.5. The total water-binder ratio was fixed as 0.25 in the proposed mixture design. Material properties of the GPC constituents are described as follows:

Class "F" low calcium fly ash was used as a binder in the GPC matrix. The quantity of fly ash used in the GPC was 60% of the total binder content by weight. The fly ash was provided by Boral Australia.[18] Ground-granulated blast-furnace slag (GGBFS) was also used as a binder in the GPC matrix. The GGBFS used in this study was provided by the Australasian Slag Association.[19] The GGBFS was 40% of the total binder content by weight. Alkaline solution was used in the GPC for activating the binders. A mixture of sodium hydroxide (NaOH) and sodium silicate solution was used as an alkaline activator in this study. The concentration of NaOH solution was 14 M.

Coarse aggregates with a maximum size of 10 mm (0.394 in.) were used. Coarse aggregates were washed and air-dried. River sand was used as fine aggregate in the mixture. A superplasticizer (high-range water-reducing admixture [HRWRA]) was provided by BASF Chemicals Australia,[20] and was used to increase the workability and the setting time of GPC. The HRWRA is based on polycarboxylate ether polymer.

Fiber-reinforced polymer (FRP)

Two types of FRP were used in the study. Basalt FRP used in this study was manufactured using 540 g/m^2 (7.6×10^{-4} lb/in.^{2}) unidirectional basalt fabric provided by the Basalt fiber tech Australia.[21] Glass FRP was manufactured using 460 g/m^2 (6.5×10^{-4} lb/in.^{2}) unidirectional E-glass fabric.

Table 1—Geopolymer concrete mixture proportions

Material	Quantity, kg/m^3
Fly ash	270
GGBFS	180
Coarse aggregates	1294
Sand	552
14 M NaOH solution	45
Na_2SiO_3	113
Water	92
HRWRA	35

Note: 1 kg/m^3 = 3.61×10^{-5} lb/in.^{3}

The tensile strength of the FRP coupons was ascertained as per ASTM D7565/D7565M-10.[22] Large pieces of fabric were cut and placed on a smooth surface for the manufacturing of FRP coupons. Epoxy resin was used with hardener in the ratio 1:5 by weight as recommended by the manufacturer.[23] Wet layup procedure was used. Resin was applied using a brush. A plastic scrapper was used to remove the extra resin from each layer. Five coupons of 300 mm (11.8 in.) length and 30 mm (1.18 in.) width of each type of FRP (that is, BFRP and GFRP) were prepared. Aluminum tabs of 70 mm (2.75 in.) length and 30 mm (1.18 in.) width with a thickness of 3 mm (0.12 in.) were glued at the edges of the FRP coupons. Two component high-strength glue was used to stick the aluminum tabs with FRP coupons. Three strain gauges of 20 mm (0.79 in.) length were installed on each FRP coupon. Two strain gauges were installed on one face of the FRP coupon. One strain gauge was installed at the center on the other face of each FRP coupon.

Tensile behavior of the FRP coupons was tested in the 500 kN (112,404.4 lb) Instron universal testing machine at the Civil Engineering High Bay Labs in the University of Wollongong, Australia. Aluminum tabs installed on the FRP coupons were clamped by the machine jaws on each edge. Tension was applied at displacement-controlled loading rate of 2 mm/minute (0.078 in./minute) as recommended by ASTM D7565/D7565M-10.[22] Readings of strain gauges were recorded continuously by a data logging system connected to the machine. Test results are presented in Table 2. The FRP sheet thickness was calculated by the properties of the fabric as provided by the manufacturer. Test results showed that the tensile strength, rupture strain, and modulus of elasticity of BFRP is higher than the GFRP. The average tensile strength of BFRP coupons was almost 60% higher than the GFRP specimens. The average modulus of elasticity of BFRP was recorded as 13.6% higher than the GFRP. Similarly, the rupture strain of BFRP was 43% higher than the GFRP. Except the rupture strain of BFRP, the coefficient of variation for all the test results was in the range from 0.95% to 2.73%. The coefficient of variation for the rupture strain of BFRP was 7.31%.

TEST MATRIX

Twenty-one GPC specimens were prepared and tested. The diameter and the height of the specimens were 153 mm (6 in.) and 306 mm (12 in.), respectively. Table 3 presents

Table 2—Average physical and mechanical properties of FRP materials

Material	GFRP	BFRP
Thickness per layer, mm	0.165	0.178
Average tensile strength, MPa	1252	2002
Coefficient of variation, %	1.72	1.06
Average modulus of elasticity, MPa	79,128	89,914
Coefficient of variation, %	2.00	0.95
Average rupture strain	0.0172	0.0246
Coefficient of variation, %	2.73	7.31

Note: 1 MPa = 145.03 psi; 1 mm = 0.0394 in.

the test matrix developed for this study. Seven groups of specimens were developed. Group "R" consisted of the reference or unconfined GPC specimens. Groups "G-2", "G-4", and "G-6" consisted of the GPC specimens confined with two, four, and six layers of GFRP, respectively. Similarly, Groups "B-2", "B-4 and "B-6" consisted of the GPC specimens confined with two, four, and six layers BFRP, respectively. Each group consists of three nominally identical specimens. The alphabet in the specimen designation shows the type of FRP confinement—that is, B for BFRP, G for GFRP, and R for reference or unconfined specimens. Numeric digit after the "-" sign shows the number of layers of FRP. Roman numerals used in the specimen designation are used to differentiate the three identical specimens in each group. For example, B-2-I is the first specimen of the group with two layers of BFRP confinement.

SPECIMENS PREPARATION

The GPC was cast and poured in the polyvinyl chloride (PVC) pipes. The PVC pipes of 153 mm (6 in.) diameter and 306 mm (12 in.) height were cut and installed on a wooden pallet to act as a mold. Sodium hydroxide pellets were mixed in water 18 to 20 hours before the concrete preparation. Almost 35 minutes before concrete mixing, alkaline solution was prepared by adding sodium silicate solution in the sodium hydroxide solution. The dry constituents were thoroughly mixed in the mixer first and then the alkaline solution was added in the mixture. After 100 seconds, water and HRWRA were added to the concrete mixture. The GPC was mixed until it became homogeneous. The slump of the prepared GPC was 116 mm (4.56 in.).

The GPC was then poured into the PVC molds and vibrated with a poker vibrator. Top of the cylinders were finished and covered with the polyethylene sheet to avoid the loss of moisture. The GPC specimens were cured at room temperature in the PVC molds. After 28 days, the PVC mold was cut and removed to get the GPC specimen out of the mold. The specimens were left at room temperature in the lab for 24 hours. Basalt and glass fiber sheets were first impregnated with the epoxy resin using a plastic scrapper. The saturated fiber sheets were then applied on the GPC cylinders. An overlap of 150 mm (6 in.) was provided during wrapping the FRP around GPC specimens to avoid debonding.

Table 3—Test matrix

Group designation	Specimen designation	FRP type	No. of layers
R	R-1	Nil	Nil
	R-2	Nil	Nil
	R-3	Nil	Nil
G-2	G-2-I	Glass	2
	G-2-II	Glass	2
	G-2-III	Glass	2
G-4	G-4-I	Glass	4
	G-4-II	Glass	4
	G-4-III	Glass	4
G-6	G-6-I	Glass	6
	G-6-II	Glass	6
	G-6-III	Glass	6
B-2	B-2-I	Basalt	2
	B-2-II	Basalt	2
	B-2-III	Basalt	2
B-4	B-4-I	Basalt	4
	B-4-II	Basalt	4
	B-4-III	Basalt	4
B-6	B-6-I	Basalt	6
	B-6-II	Basalt	6
	B-6-III	Basalt	6

INSTRUMENTATION

For each cylinder specimen, two linear variable displacement transducers (LVDT) were placed between the platens of the compression testing machine. Additionally, a compressometer with four LVDTs was also used to measure the axial deformation. The compressometer with LVDTs was centered at the midheight of the cylinder with a gauge length of 166 mm (6.53 in.). For each cylinder wrapped with FRP, three strain gauges were placed at the midheight of the cylinder in the hoop direction to measure the circumferential strain. The strain gauges used were of 20 mm (0.787 in.) gauge length. The strain gauges were placed 90 degrees apart from each other along the circumference outside the overlapping zone. Figure 1 shows a typical instrumented test specimen.

AXIAL COMPRESSION TEST

Axial compression test on the prepared specimens was conducted as per AS 1012.9-2014.[24] A compression testing machine with a loading capacity of 5000 kN (1,124,044.7 lb) was used for the test. A displacement-controlled load at a rate of 0.2 mm/minute (0.0078 in./minute) was applied. All the LVDTs and strain gauges were connected to a data logging system to record the readings continuously.

RESULTS AND DISCUSSION

Test results are tabulated in Table 4. Failure modes, stress-strain behavior, effect of type of FRP on axial compressive strength, effect of number of FRP layers on compressive

strength, effect of FRP type on ultimate axial strain, and effect of number of FRP layers on ultimate axial strain of the specimens are discussed in the following.

Failure modes

Typical failure modes for all the groups of specimens tested are presented in Fig. 2. Figure 2(a) shows the failure mode of unconfined or reference specimen. In the unconfined GPC specimen, localized microcracks were initiated and resulted in the complete failure of the specimen at peak load. All the FRP confined GPC specimens failed due to the rupture of FRP at the mid-height of the specimen with a loud noise. This behavior is quite similar to the FRP-confined OPC.

Figure 2(b) to (g) shows the typical failure mode of the FRP-confined GPC specimens. For all the FRP-confined GPC specimens, light cracking sounds were heard before the complete rupture. Those light sounds were the indication of the localized cracking of the FRP jacket and those localized cracks then led to the development of a large crack with a loud noise. The duration of these slight noises was longer for the BFRP-confined specimens than the GFRP-confined specimens.

Stress-strain behavior

Figures 3 and 4 show the axial stress-strain behavior of all the specimens confined with GFRP and BFRP, respectively. Typical axial stress-axial strain behavior of unconfined or reference specimen is also shown in both the figures for comparison. It can be observed that except Groups G-2 and B-2, all the GFRP- and BFRP-confined specimens showed a strain-hardening response. This is due to the lower confinement pressures of Group G-2 and B-2.

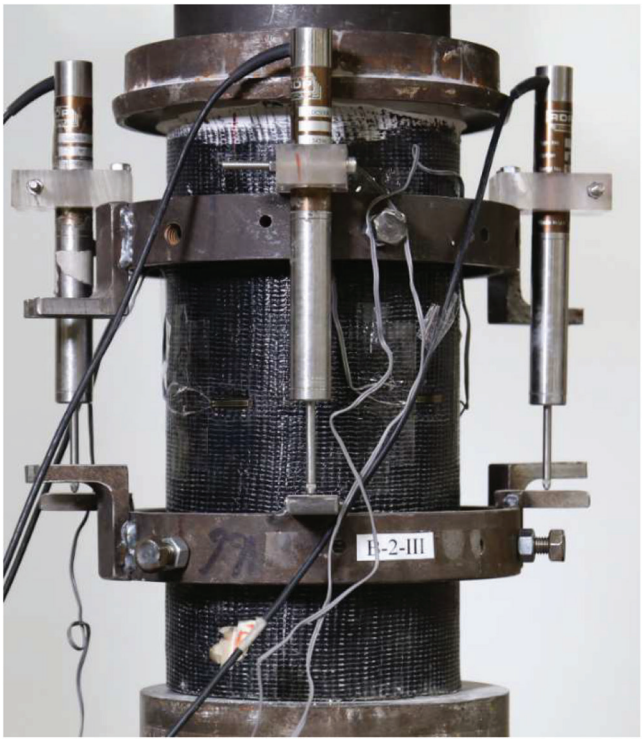

Fig. 1—Typical instrumented test specimens.

Table 4—Test results of axial compression tests

Group ID	Specimen ID	f_{co}', MPa	ε_{co}, %	f_{cc}', MPa	ε_{cu}, %	$\varepsilon_{h,rup}$, %	f_l, MPa	f_{cc}'/f_{co}	f_{cc}'/f_l	$\varepsilon_{cu}/\varepsilon_{co}$
R	R-I	44.31	0.33	—	—	—	—	—	—	—
	R-II	48.99	0.37	—	—	—	—	—	—	—
	R-III	45.58	0.32	—	—	—	—	—	—	—
G-2	G-2-I	46.29	0.34	56.2	0.67	0.73	5.9	1.21	9.57	1.95
	G-2-II			55.6	0.83	0.76	5.9	1.20	9.46	2.41
	G-2-III			57.9	0.77	0.71	5.9	1.25	9.85	2.21
G-4	G-4-I	46.29	0.34	62.8	1.17	1.59	11.8	1.36	5.34	3.38
	G-4-II			67.4	1.18	1.47	11.8	1.46	5.73	3.41
	G-4-III			67.6	0.96	1.51	11.8	1.46	5.75	2.76
G-6	G-6-I	46.29	0.34	87.1	1.33	1.63	17.6	1.88	4.94	3.84
	G-6-II			90.2	1.30	1.69	17.6	1.95	5.12	3.75
	G-6-III			85.8	1.16	1.61	17.6	1.85	4.86	3.35
B-2	B-2-I	46.29	0.34	57.0	1.18	1.72	10.3	1.23	5.52	3.40
	B-2-II			54.3	0.94	1.69	10.3	1.17	5.26	2.72
	B-2-III			55.1	1.18	1.71	10.3	1.19	5.34	3.42
B-4	B-4-I	46.29	0.34	79.6	1.72	1.44	20.7	1.72	3.85	4.95
	B-4-II			80.2	1.30	1.47	20.7	1.73	3.88	3.75
	B-4-III			84.5	1.50	1.70	20.7	1.82	4.09	4.32
B-6	B-6-I	46.29	0.34	106.7	2.27	1.81	31.0	2.30	3.44	6.55
	B-6-II			113.2	2.47	1.91	31.0	2.45	3.65	7.13
	B-6-III			112.1	2.49	1.76	31.0	2.42	3.62	7.19

Note: 1 MPa = 145.03 psi.

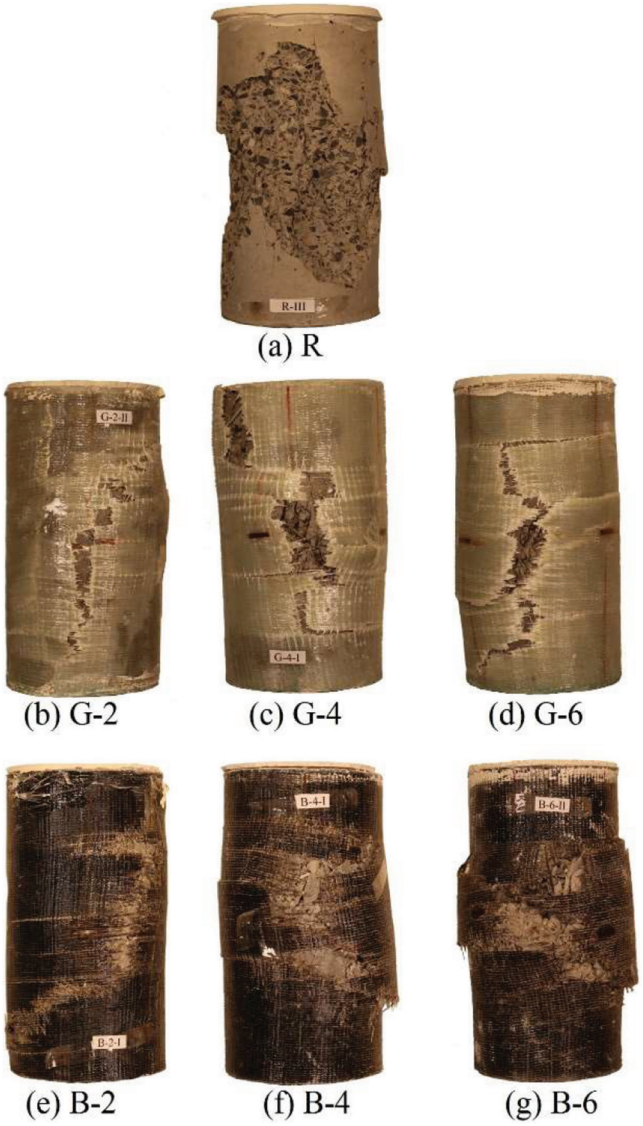

Fig. 2—Typical failure modes of all groups.

Figure 5 shows the comparison of stress-strain curves of Groups G-6 and B-6. It can be observed that both Groups G-6 and B-6 shows a bilinear strain hardening response. There are two distinct regions of the stress-strain curve: first nonlinear region based on the modulus of elasticity of the GPC and second linear region based on FRP confinement effectiveness. There is a transition region between the two regions and can be defined as the region where the curve changes the slope. Figure 5 also shows that both the groups—that is, G-6 and B-6—have the same slope of the first region and a similar transition region. The slope of the second region is also similar for both the groups but the peak points are different. Group G-6 showed lower peak strength and ultimate strain than Group B-6. This is due to the lower tensile strength and rupture strain of the GFRP as compared to the BFRP.

Figure 6 shows the comparison of stress-strain curves of Groups G-4 and B-4. It can be observed that the stress-strain curves of both the groups showed three regions. The first nonlinear region is similar to that of Groups G-6 and B-6. After that, there is a transition region where the axial strain increased but the strength increase was not observed. For

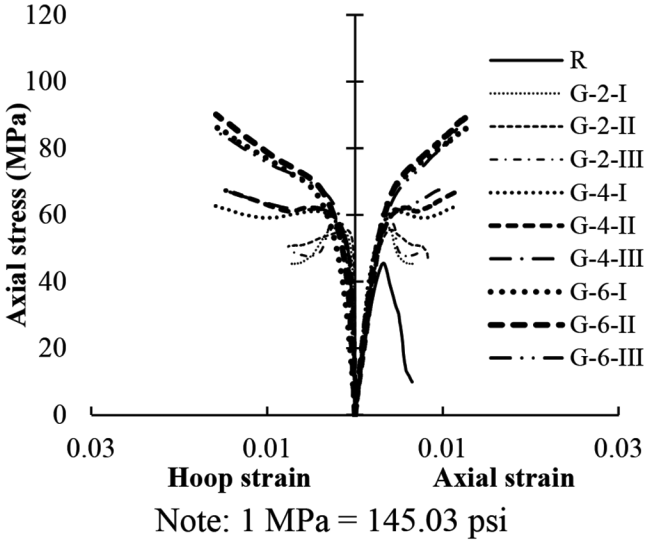

Fig. 3—Axial and lateral stress-strain response of GFRP-confined GPC specimens.

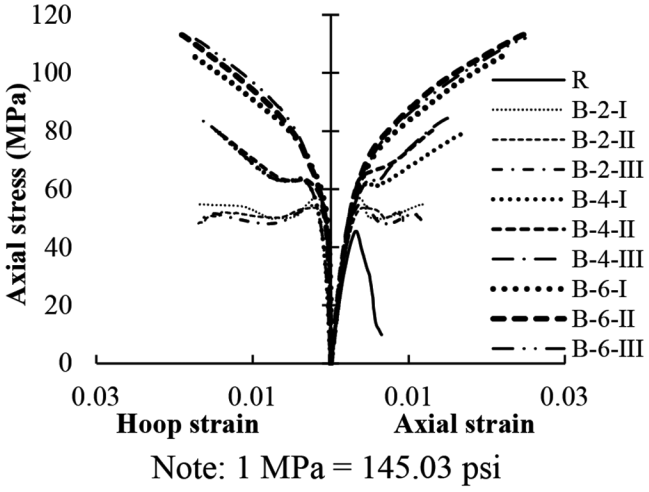

Fig. 4—Axial and lateral stress-strain response of BFRP-confined GPC specimens.

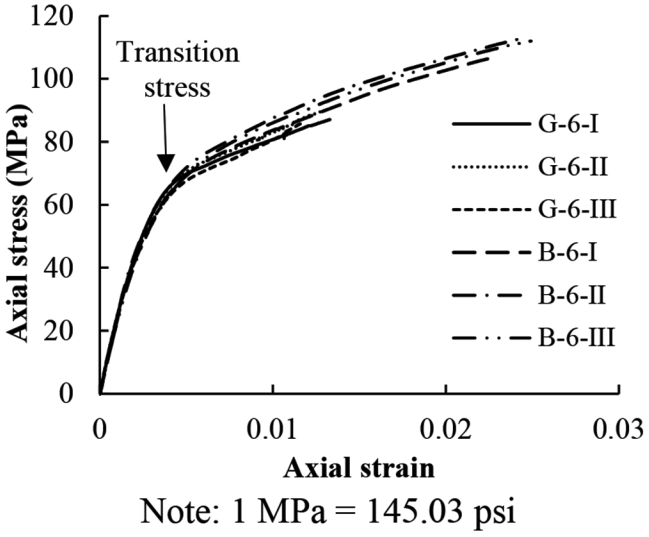

Fig. 5—Stress-strain curves of Groups G-6 and B-6.

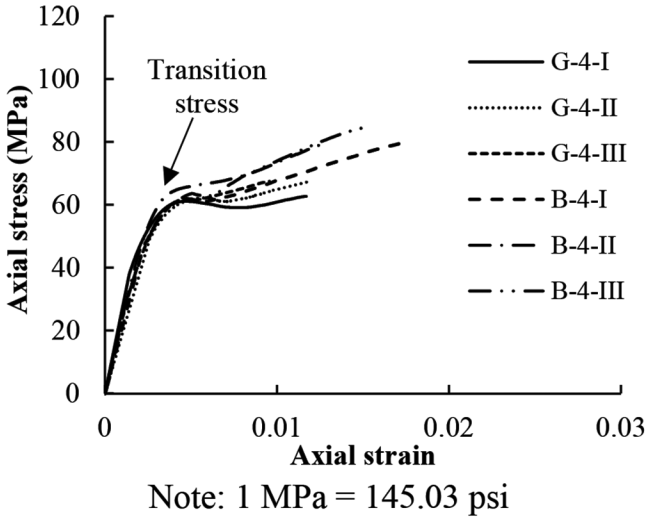

Fig. 6—Stress-strain curves of Groups G-4 and B-4.

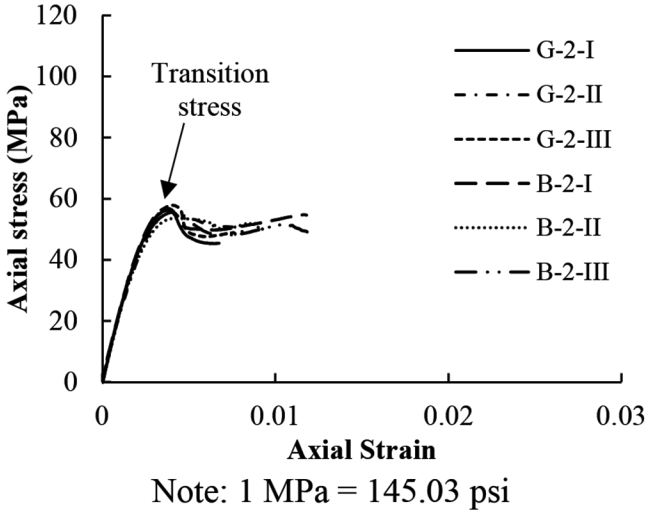

Fig. 7—Stress-strain curves of Groups G-2 and B-2.

some of the specimens, the stress even decreased in this region. This can be due to the disintegration of the confined GPC and readjustment of stresses between the GPC and the external FRP confinement. In the third region of stress-strain curves, the slope of the curve increased as compared to the second region and stress increase is observed with the increase in strain. In this region, the FRP confinement became active and successfully confined the GPC until the rupture of FRP.

Figure 7 shows the comparison of stress-strain curves of Groups G-2 and B-2. It can be observed that both the groups resulted in stress-strain curves with strain softening response. The latter can be defined as the response of the stress-strain curve where the ultimate stress of FRP-confined concrete is lower than the peak stress of FRP-confined concrete. There are three regions of the stress strain curves of both the groups: 1) first nonlinear region based on the modulus of elasticity of GPC; 2) second transition region, where the peak stress of the FRP-confined GPC is observed and after that the stress decreased; and 3) third region after the transition region where the stress is approximately constant or experienced a slight decrease with increase in strain until the rupture point of FRP.

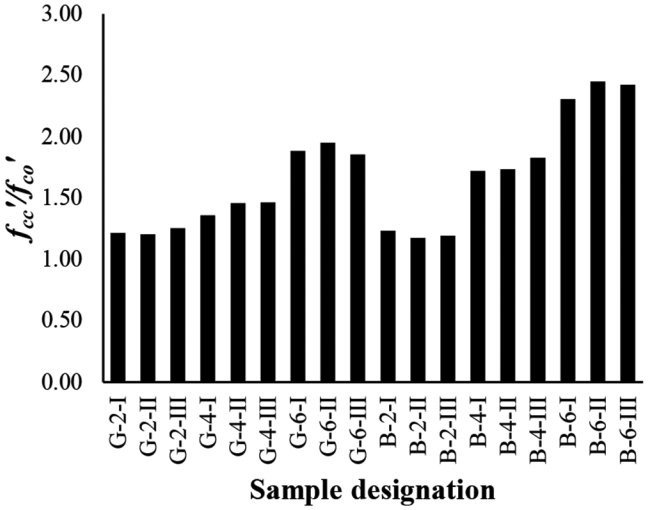

Fig. 8—Confinement effectiveness of test specimens.

Typical behavior of the stress-strain curve for the presented results is similar to the FRP-confined OPC. The major difference observed is the transition stress after the first region. The transition stress can be defined as the stress at which the slope of the curve starts to change significantly. The approximate transition stress locations for all the curves were highlighted in Fig. 5 through 7. In FRP-confined OPC, the transition stress occurs approximately near the peak stress of unconfined concrete. However, in the present study, it is observed that in FRP-confined GPC, this transition stress is higher than unconfined GPC strength. Similar stress-strain behavior was observed by Oliveira et al.[25] for FRP confined high-strength OPC. This shows that the stress-strain behavior of the FRP-confined normal-strength GPC is similar to the FRP-confined high-strength OPC. Also, Lokuge and Karunasena[14] observed that the stress-strain behavior of FRP-confined GPC was similar to the FRP-confined high-strength OPC. This phenomenon was not observed for the geopolymer concrete-filled FRP tubes as reported by Ozbakkaloglu and Xie.[15] This difference in the behavior is believed to be at least partially due to the unconfined geopolymer concrete strength. The strength of the GPC reported in Ozbakkaloglu and Xie[15] was approximately 25 MPa (3625 psi) and the compressive strength of the GPC used in this study is in the range of 44 to 49 MPa (6381 to 7106 psi).

Effect of type of FRP on compressive strength

Both the types of FRP used in the study resulted in the increase of the compressive strength of the GPC. Figure 8 shows the strength enhancement in terms of f_{cc}'/f_{co}'. Terms f_{cc}' and f_{co}' are the peak compressive stress of confined GPC and unconfined GPC, respectively. It can be observed that Group B-2 resulted in the least strength enhancement and Group B-6 resulted in the highest strength enhancement.

Groups G-2 and B-2 resulted in 22% and 19% average increase in GPC strength, respectively. Despite the lower confinement pressure, Group G-2 resulted in higher increase as compared to Group B-2. This can be due to the scatter of the test results. Groups G-4 and B-4 resulted in 42% and 75% average increase in GPC strength, respectively. Groups

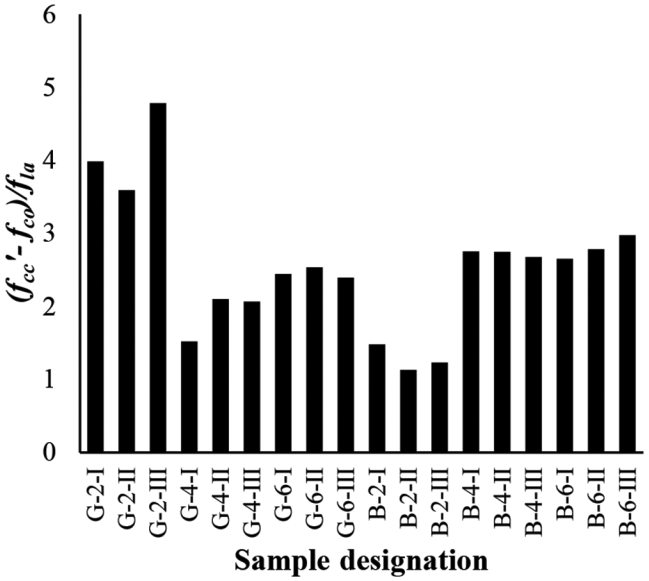

Fig. 9—Confinement effectiveness in comparison with confinement pressure for tested specimens.

G-6 and B-6 resulted in 89% and 139% average increase in GPC strength, respectively. This can be due to the higher elastic modulus and rupture strain of BFRP than GFRP.

Term f_{la} is known as the actual maximum confinement pressure provided by the FRP and can be determined using Eq. (1). The maximum confinement pressure f_l can be determined by replacing the hoop rupture strain of FRP in Eq. (1) with the ultimate tensile strain of FRP in coupon test.

$$f_{la} = \frac{2E_{frp}t\varepsilon_{h,avg}}{D} \quad (1)$$

where f_{la} is the actual maximum confinement pressure; E_{frp} is modulus of elasticity of FRP; t is thickness of FRP; $\varepsilon_{h,avg}$ is the average hoop rupture strain of FRP; and D is diameter of the specimen.

Figure 9 shows the confinement effectiveness in relation to the confinement pressure $(f_{cc}' - f_{co})/f_{la}$ for all the specimens. It can be observed that despite the fact that Group B-2 has higher confinement pressure (f_{la}), the strength enhancement is more in Group G-2. The groups with a greater number of layers—that is, higher confinement pressure (f_{la})—shows the opposite behavior. It can be observed from Fig. 9 that Groups B-4 and B-6 showed the higher confinement effectiveness than Groups G-4 and G-6, respectively. This is an indication that leads to the observation that BFRP confinement on geopolymer concrete resulted in a higher strength enhancement than the GFRP confinement, which might be attributed to the higher modulus of elasticity and rupture strain of BFRP than GFRP.

Effect of number of FRP layers on compressive strength

Generally, the increase in number of layers of FRP confinement on concrete increases the compressive strength. The same was observed for FRP confinement on GPC. Average compressive strength of Groups G-4 and G-6 is 16% and 54% higher than Group G-2. Similarly, average compressive strength of Groups B-4 and B-6 is 46% and 99% higher than Group B-2. This shows that the increase in compressive strength with the number of FRP layers is more pronounced for BFRP confinement on GPC than GFRP confinement on GPC. This can be due to the higher tensile strength and rupture strain of BFRP as compared to GFRP.

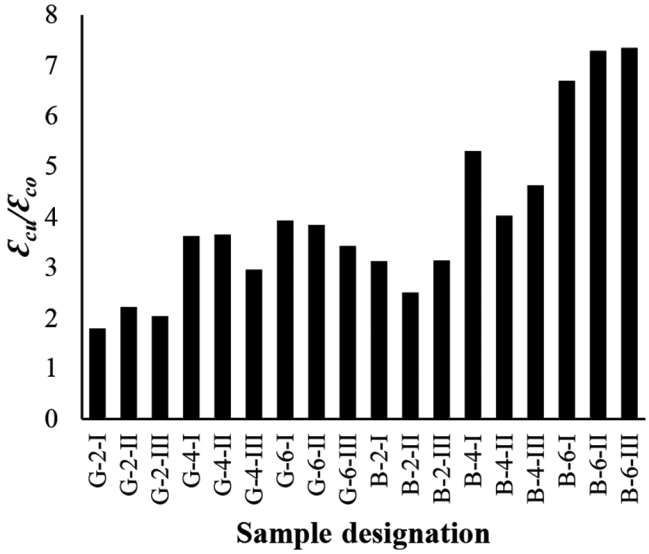

Fig. 10—Axial strain enhancement of tested specimens.

Effect of FRP type on ultimate axial strain

Both GFRP and BFRP confinement resulted in the increase in ultimate axial compressive strain of FRP confined GPC than the unconfined GPC. Strain enhancement ratio ($\varepsilon_{cu}/\varepsilon_{co}$), which is defined as the ratio of ultimate strain of FRP confined GPC (ε_{cu}) to the strain of unconfined GPC at peak stress (ε_{co}), is plotted in Fig. 10 for all the specimens. It can be observed that Group G-2 resulted in the least strain enhancement and Group B-6 resulted in the highest strain enhancement. This observation can be supported by the fact that the BFRP has higher rupture strain than GFRP, which leads to the delay in the FRP jacket rupture and enhancement of axial strain. The hoop rupture strains of the FRP-confined GPC are lower than their ultimate tensile rupture strain. According to ACI 440.2R,[26] this is due to the existence of a multiaxial stress state in case of FRP confined concrete as compared to the FRP coupon tensile test.

Groups G-2 and B-2 resulted in 119% and 218% average increase in average strain at peak stress of unconfined GPC, respectively. Similarly, Groups G-4, B-4, G-6, and B-6 resulted in 218%, 334%, 264%, and 595% increase in average strain at peak stress of unconfined GPC, respectively. It can be observed that Group B-4 shows the higher strain enhancement than Group G-6. This shows that BFRP confinement is more effective in increasing the ultimate axial strain of the FRP-confined GPC than the GFRP confinement. This can be due to the higher rupture strain of BFRP than GFRP.

Effect of number of FRP layers on ultimate axial strain

Average ultimate axial strains of Groups G-4 and G-6 are 45% and 66% higher than the average ultimate axial strain of

Table 5—Comparison of predicted peak axial compressive stress by existing models with experimental

Group	Specimen	Experimental f_{cc}', MPa	Predicted f_{cc}' by existing confinement models for FRP-confined normal concrete, MPa									
			Karbhari and Gao[32]	Samaan et al.[33]	Cheng et al.[34]	Lam and Teng[27]	Wu et al.[35]	Berthet et al.[29]	Tamuzs et al.[36]	Youssef et al.[28]	Benzaid et al.[37]	Wei and Wu[38]
G-2	G-2-I	56	61	66	59	55	58	55	60	53	50	61
	G-2-II	56	61	66	59	55	58	55	60	53	50	61
	G-2-III	58	61	66	59	54	58	55	60	53	50	61
G-4	G-4-I	63	74	78	72	82	70	84	74	63	64	74
	G-4-II	67	74	78	72	79	70	81	74	63	62	74
	G-4-III	68	74	78	72	80	70	82	74	63	63	74
G-6	G-6-I	87	85	88	85	101	82	104	89	74	73	87
	G-6-II	90	85	88	85	103	82	106	89	74	74	87
	G-6-III	86	85	88	85	101	82	103	89	74	73	87
B-2	B-2-I	57	70	75	69	70	67	71	71	60	58	71
	B-2-II	54	70	75	69	70	67	71	71	60	58	71
	B-2-III	55	70	75	69	70	67	71	71	60	58	71
B-4	B-4-I	80	90	93	91	86	88	88	96	80	66	94
	B-4-II	80	90	93	91	87	88	89	96	80	66	94
	B-4-III	84	90	93	91	93	88	96	96	80	69	94
B-6	B-6-I	107	109	108	114	122	108	125	120	102	83	116
	B-6-II	113	109	108	114	126	108	129	120	102	85	116
	B-6-III	112	109	108	114	119	108	123	120	102	82	116
Average absolute error, %			11	15	9	15	8	17	13	7	13	12

Note: 1 MPa = 145.03 psi

Group G-2. Similarly, average ultimate axial strains of Groups B-4 and B-6 are 36% and 118% higher than the average ultimate axial strain of Group B-2. This shows that the increase in strain enhancement with the increase in the number of FRP layers is more pronounced in the case of BFRP confinement on GPC than the GFRP confinement on GPC.

COMPARISON WITH EXISTING CONFINEMENT MODELS OF FRP-CONFINED NORMAL CONCRETE

Peak axial compressive stress

Several stress-strain models have been proposed for FRP-confined normal concrete.[26-28] Most of the proposed models are capable to predict the ultimate conditions of the FRP-confined normal concrete. In this part of the study, the experimental test results for peak compressive stress of FRP-confined GPC were compared with the existing models for FRP confined OPC, as shown in Table 5.

The average absolute error (AAE) was also calculated and tabulated in Table 5 for each model. A comparison of prediction accuracy of peak axial compressive stress with each confinement model is shown in Fig. 11(a). It can be observed that among all the tested models, Youssef et al.[28] is the best performing model for the prediction of peak axial compressive stress of FRP confined GPC. Also, Berthet et al.[29] is the least accurate among all the tested models.

Axial strain at peak compressive stress

Models for FRP-confined normal concrete also provide the prediction of axial strain at peak compressive stress. The

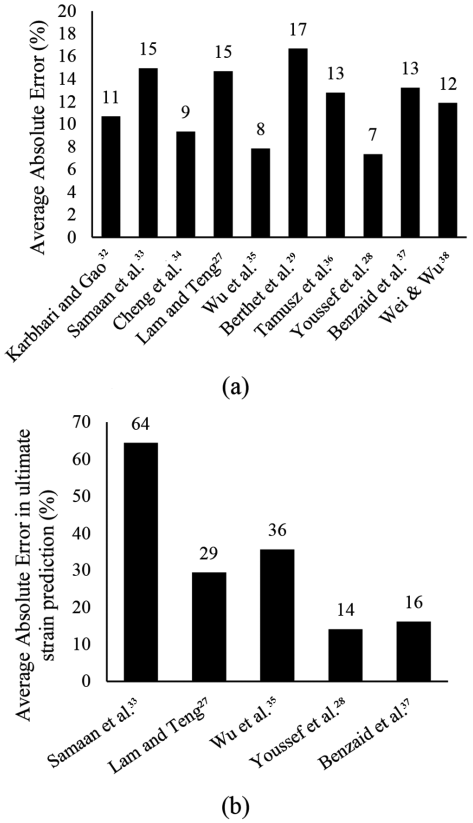

Fig. 11—Comparison of average absolute error in prediction of existing confinement models for: (a) peak axial compressive stress; and (b) axial compressive strain at peak stress.

Table 6—Comparison of predicted peak axial strain by existing models with experimental

Group	Specimen	Experimental ε_{cc}', %	Predicted ε_{cc}' by existing confinement models for FRP confined normal concrete, %				
			Samaan et al.[33]	Lam and Teng[27]	Wu et al.[35]	Youssef et al.[28]	Benzaid et al.[37]
G-2	G-2-I	0.67	1.00	0.82	0.79	0.72	0.83
	G-2-II	0.83	0.92	0.83	0.79	0.72	0.84
	G-2-III	0.77	1.22	0.81	0.79	0.72	0.83
G-4	G-4-I	1.17	1.24	1.53	1.24	1.10	1.31
	G-4-II	1.18	1.70	1.46	1.24	1.10	1.26
	G-4-III	0.96	1.71	1.48	1.24	1.10	1.28
G-6	G-6-I	1.33	2.83	2.03	1.62	1.48	1.64
	G-6-II	1.30	3.08	2.08	1.62	1.48	1.68
	G-6-III	1.16	2.72	2.01	1.62	1.48	1.63
B-2	B-2-I	1.18	0.85	1.33	1.63	1.12	1.10
	B-2-II	0.94	0.52	1.32	1.63	1.12	1.10
	B-2-III	1.18	0.62	1.32	1.63	1.12	1.10
B-4	B-4-I	1.72	2.38	1.81	2.58	1.90	1.38
	B-4-II	1.30	2.44	1.84	2.58	1.90	1.39
	B-4-III	1.50	2.83	2.03	2.58	1.90	1.50
B-6	B-6-I	2.27	3.61	2.88	3.37	2.69	1.99
	B-6-II	2.47	4.25	2.89	3.26	2.57	1.99
	B-6-III	2.49	4.00	2.82	3.37	2.69	1.95
Average absolute error, %			77	36	39	16	19

experimental test results for axial strain at peak compressive stress of FRP-confined GPC were compared with the existing models for FRP-confined normal concrete. Table 6 shows the comparison of experimental axial strain at peak compressive stress for FRP-confined GPC with the values of the same as predicted by different existing confinement models for FRP confined normal concrete.

A comparison of prediction accuracy of axial strain at peak compressive stress with each confinement model is shown in Fig. 11(b). It can be observed that among all the tested models, Youssef et al.[28] is the best performing model for the prediction of axial strain at peak compressive stress of FRP-confined GPC.

Lateral strain-axial strain curves

Lateral strain-axial strain relationship is an important parameter in the analysis-oriented confinement models.[30] Figure 12 shows the experimental lateral strain-axial strain curves of the tested specimens. The experimental curves were compared with the lateral strain-axial strain curves predicted for each group by Jiang and Teng[31] for FRP-confined OPC. Jiang and Teng[31] presented Eq. (2) as the lateral strain-axial strain relationship for FRP-confined OPC.

$$\Phi\left(\frac{-\varepsilon_l}{\varepsilon_{co}}\right)=\frac{\varepsilon_c}{\varepsilon_{co}}\Big/\left(1+8\frac{o_l'}{f_{co}'}\right)$$
$$=0.85\left\{\left[1+0.75\left(\frac{-\varepsilon_l}{\varepsilon_{co}}\right)\right]^{0.7}-exp\left[-7\left(\frac{-\varepsilon_l}{\varepsilon_{co}}\right)\right]\right\} \quad (2)$$

where ε_c is strain of confined concrete at any particular confinement pressure; ε_{co} is strain at peak stress of unconfined concrete; ε_l is lateral strain = $-\varepsilon_h$; f_{co}' is peak stress of unconfined concrete; o_l' is lateral confinement pressure = $E_{frp}t\varepsilon_h/R$; E_{frp} is modulus of elasticity of FRP; t is thickness of FRP; ε_h is hoop strain of FRP in confined concrete; R is radius of concrete specimen.

It can be observed from Fig. 12 that the prediction accuracy of the relationship proposed by Jiang and Teng[31] is higher for the groups with lower confinement pressure than the other groups of same FRP type.

Stress-strain curves

Stress-strain curves for FRP-confined normal concrete can be predicted with the existing confinement models available. It should be noted that currently there is no confinement model available to predict the stress-strain curve of FRP-confined GPC. Models proposed for the FRP-confined normal concrete were used to predict the stress-strain curves of FRP-confined GPC in this study. The predicted stress-strain curves were compared with the experimental stress-strain curves to determine the applicability of existing confinement models for FRP-confined OPC to the FRP-confined GPC. From Fig. 11, it can be observed that Youssef et al.[28] is the best performing confinement model among all the tested models with least average absolute error in the prediction of ultimate conditions of FRP-confined GPC. Therefore, stress-strain behavior of FRP-confined GPC predicted by Youssef et al.[28] was compared with the experimental stress-strain curve. Also, an analysis-oriented model proposed by

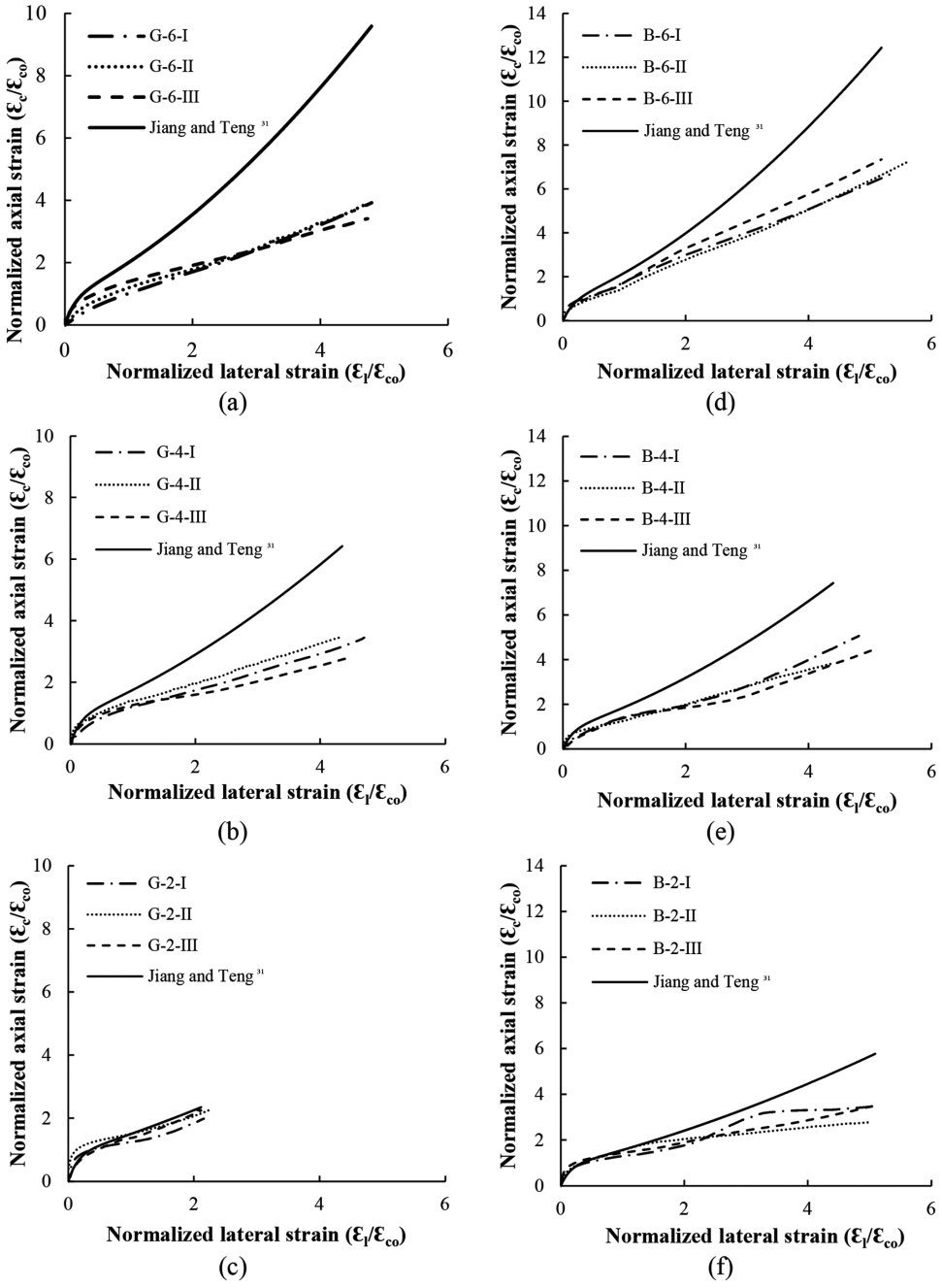

Fig. 12—Comparison of experimental and model-predicted lateral strain-axial strain curves of Groups: (a) G-6; (b) G-4; (c) G-2; (d) B-6; (e) B-4; and (f) B-2. (Note: 1 MPa = 145.03 psi.)

Jiang and Teng[31] for FRP-confined OPC was selected to compare the experimental stress-strain curves.

Figure 13 shows the comparison of experimental stress-strain curves for FRP-confined GPC with the stress-strain curves predicted by the Youssef et al.[28] and Jiang and Teng.[31] It can be observed that the stress-strain curves predicted by the existing models are close to the experimental stress-strain curves for the specimens with low confinement pressure. For the specimens with higher confinement pressure, the existing models are unable to predict the behavior of FRP-confined GPC. Also, it can be observed again that the stress-strain curves of FRP-confined GPC concrete exhibited a higher transition stress.

It can be observed that confinement model proposed by Youssef et al.[28] is capable to predict the ultimate conditions of the FRP-confined GPC to a better extent than the model proposed by Jiang and Teng.[38] Validation of this fact cannot be performed as there is no database related to FRP-confined GPC with an unconfined GPC strength in the range of 40 to 50 MPa (5800 to 7250 psi) is available.

CONCLUSIONS

The following conclusions are drawn based on the results and discussion:

1. The same number of layers of BFRP confinement on GPC resulted in higher peak stress and strain than GFRP confinement. This is due to the higher mechanical properties and thickness of the BFRP. However, the increase in peak compressive stress with respect to the confinement pressure

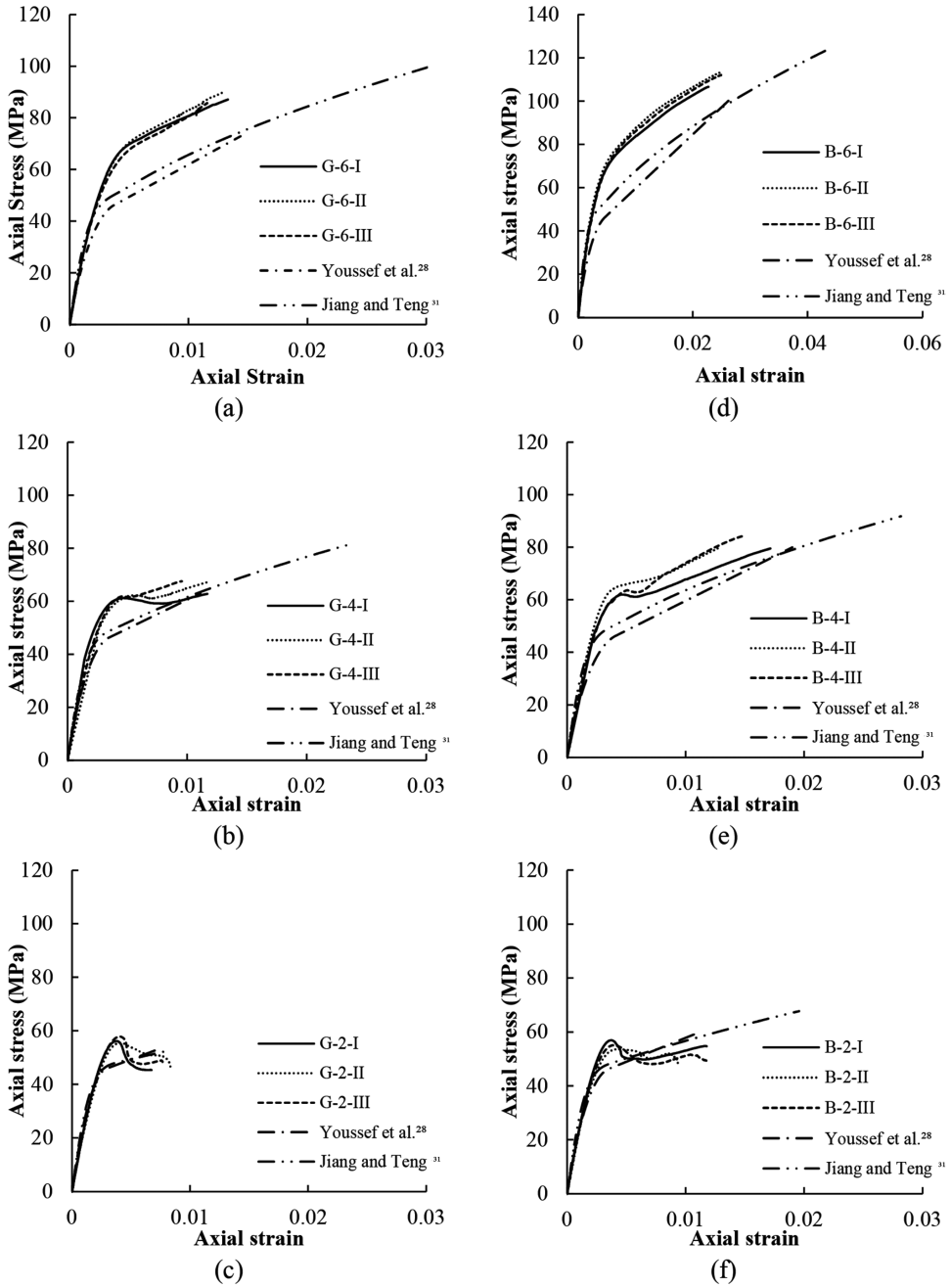

Fig. 13—Comparison of experimental and model-predicted axial stress-strain curves of Groups: (a) G-6; (b) G-4; (c) G-2; (d) B-6; (e) B-4; and (f) B-2.

was higher for BFRP confinement than GFRP confinement on GPC.

2. Basalt fiber-reinforced polymer confinement is superior than GFRP confinement as it is based on a natural mineral fiber and has better mechanical properties than GFRP. Therefore, BFRP-confined GPC is presented as a proposed solution to the sustainability challenges in construction industry.

3. Fiber-reinforced polymer-confined GPC stress-strain behavior is different than the FRP-confined OPC. A higher transition stress can be observed in FRP-confined GPC.

4. Existing confinement models for FRP-confined OPC may be used to predict the peak axial stress and strain at peak stress but are unable to accurately predict the stress-strain behavior of FRP-confined GPC.

Further research needs to be conducted on the development of a confinement model for FRP-confined geopolymer concrete.

AUTHOR BIOS

Junaid Ahmad *is a PhD Candidate in the School of Civil, Mining and Environmental Engineering at the University of Wollongong, NSW, Australia. He received his BSc in civil engineering and MS in structural engineering from the University of Engineering and Technology, Taxila, Pakistan, in 2010 and 2015, respectively. He is also a Lecturer at National University of Sciences and Technology (NUST), Islamabad, Pakistan. His research interests include use of geopolymer concrete in structural members.*

Tao Yu *is a Professor in the Department of Civil and Environmental Engineering at The Hong Kong Polytechnic University, Hong Kong. He received his BEng from Zhejiang University, China, in 2001 and his PhD from The Hong Kong Polytechnic University, Hong Kong, in 2007. His research*

interests include emerging structural materials and systems, including the infrastructure application of composite materials.

ACI member **Muhammad N. S. Hadi** *is an Associate Professor in the School of Civil, Mining and Environmental Engineering at the University of Wollongong. He received his BSc and MS from the University of Baghdad, Baghdad, Iraq, in 1977 and 1980, respectively, and his PhD from the University of Leeds, Leeds, UK, in 1989. His research interests include analysis and design of concrete structures.*

ACKNOWLEDGMENTS

The authors would like to acknowledge the Basalt fiber tech Australia for providing the basalt fabric, Boral Australia for providing the fly ash, Australasian Slag Association (ASA) for providing the GGBFS, and BASF chemicals Australia for providing the superplasticizer for the study. Also special thanks to R. Mclean and D. Best for their support during experimental work at Civil Engineering High Bay Labs, University of Wollongong, Australia. The first author acknowledges the Higher Education Commission (HEC) Pakistan and University of Wollongong, Australia, for his PhD scholarship support.

REFERENCES

1. Hardjito, D.; Wallah, S. E.; Sumajouw, D. M.; and Rangan, B. V., "On the Development of Fly Ash-Based Geopolymer Concrete," *ACI Materials Journal*, V. 101, No. 6, Nov.-Dec. 2004, pp. 467-472.

2. Ali, S.; Sheikh, M. N.; Sargeant, M.; and Hadi, M. N. S., "Influence of Polypropylene and Glass Fibers on Alkali- Activated Slag/Fly Ash Concrete," *ACI Structural Journal*, V. 117, No. 4, July 2020, pp. 183-192.

3. Sarker, P. K.; Haque, R.; and Ramgolam, K. V., "Fracture Behaviour of Heat Cured Fly Ash Based Geopolymer Concrete," *Materials & Design*, V. 44, 2013, pp. 580-586. doi: 10.1016/j.matdes.2012.08.005

4. Al-Azzawi, M.; Yu, T.; and Hadi, M. N. S., "Factors Affecting the Bond Strength between the Fly Ash-Based Geopolymer Concrete and Steel Reinforcement," *Structures*, V. 14, 2018, pp. 262-272. doi: 10.1016/j.istruc.2018.03.010

5. Farhan, N. A.; Sheikh, M. N.; and Hadi, M. N. S., "Behavior of Ambient-Cured Geopolymer Concrete Columns under Different Loads," *ACI Structural Journal*, V. 115, No. 5, Sept. 2018, pp. 1419-1429. doi: 10.14359/51702250

6. Steinerova, M.; Matulova, L.; Vermach, P.; and Kotas, J., "The Brittleness and Chemical Stability of Optimized Geopolymer Composites," *Materials (Basel)*, V. 10, No. 4, 2017, p. 396 doi: 10.3390/ma10040396

7. Pan, Z.; Sanjayan, J. G.; and Rangan, B. V., "Fracture Properties of Geopolymer Paste and Concrete," *Magazine of Concrete Research*, V. 63, No. 10, 2011, pp. 763-771. doi: 10.1680/macr.2011.63.10.763

8. Noushini, A.; Aslani, F.; Castel, A.; Gilbert, R. I.; Uy, B.; and Foster, S., "Compressive Stress-Strain Model for Low-Calcium Fly Ash-Based Geopolymer and Heat-Cured Portland Cement Concrete," *Cement and Concrete Composites*, V. 73, 2016, pp. 136-146. doi: 10.1016/j.cemconcomp.2016.07.004

9. Raffoul, S.; Escolano-Margarit, D.; Garcia, R.; Guadagnini, M.; and Pilakoutas, K., "Constitutive Model for Rubberized Concrete Passively Confined with FRP Laminates," *Journal of Composites for Construction*, ASCE, V. 23, No. 6, 2019, p. 04019044 doi: 10.1061/(ASCE)CC.1943-5614.0000972

10. Hadi, M. N. S.; Ahmad, J.; and Yu, T., "Tests of Geopolymer Concrete Columns with Basalt-Fibre-Reinforced-Polymer Bars And Tubes," *Proceedings of the Institution of Civil Engineers – Structures and Buildings*, 2020, doi: 10.1680/jstbu.19.00227.10.1680/jstbu.19.00227

11. Shi, J.; Wang, X.; Ding, L.; and Wu, Z., "Degradation of Creep Behaviors of Basalt Fiber Reinforced Polymer Tendons in Salt Solution," *Journal of Materials in Civil Engineering*, ASCE, V. 30, No. 12, 2018, p. 04018317 doi: 10.1061/(ASCE)MT.1943-5533.0002525

12. Sim, J.; Park, C.; and Moon, D. Y., "Characteristics of Basalt Fiber as a Strengthening Material for Concrete Structures," *Composites. Part B, Engineering*, V. 36, No. 6-7, 2005, pp. 504-512. doi: 10.1016/j.compositesb.2005.02.002

13. Ouyang, L. J.; Gao, W. Y.; Zhen, B.; and Lu, Z. D., "Seismic Retrofit of Square Reinforced Concrete Columns Using Basalt and Carbon Fiber-Reinforced Polymer Sheets: A Comparative Study," *Composite Structures*, V. 162, 2017, pp. 294-307. doi: 10.1016/j.compstruct.2016.12.016

14. Lokuge, W., and Karunasena, W., "Ductility Enhancement of Geopolymer Concrete Columns Using Fibre-Reinforced Polymer Confinement," *Journal of Composite Materials*, V. 50, No. 14, 2016, pp. 1887-1896. doi: 10.1177/0021998315597553

15. Ozbakkaloglu, T., and Xie, T., "Geopolymer Concrete-Filled FRP Tubes: Behavior of Circular and Square Columns under Axial Compression," *Composites. Part B, Engineering*, V. 96, 2016, pp. 215-230. doi: 10.1016/j.compositesb.2016.04.013

16. Ozbakkaloglu, T., and Lim, J. C., "Axial Compressive Behavior of FRP-Confined Concrete: Experimental Test Database and a New Design-Oriented Model," *Composites. Part B, Engineering*, V. 55, 2013, pp. 607-634. doi: 10.1016/j.compositesb.2013.07.025

17. Hadi, M. N. S.; Farhan, N. A.; and Sheikh, M. N., "Design of Geopolymer Concrete with GGBFS at Ambient Curing Condition Using Taguchi Method," *Construction and Building Materials*, V. 140, 2017, pp. 424-431. doi: 10.1016/j.conbuildmat.2017.02.131

18. Fly Ash (Bagged), https://www.boral.com.au/products/cementitious-materials/fly-ash/fly-ash-bagged, 2019 (last accessed Jan. 18, 2021).

19. Australasian (Iron & Steel) Slag Association (ASA), Ground Granulated Blast Furnace Slag (GGBFS), http://www.asa-inc.org.au/products/ground-granulated-blast-furnace-slag, 2019. (last accessed Jan. 18, 2021)

20. BASF Chemicals Australia, MasterGlenium SKY 8700, https://www.master-builders-solutions.basf.com.au/en-au/products/mastergleniumsky/masterglenium-sky-8700, 2019. (last accessed Jan. 18, 2021).

21. Basalt Fiber Tech Australia, Basalt fiber fabrics, 2015. http://www.basaltft.com/products/fab.htm, 2019. (last accessed Jan. 18, 2021)

22. ASTM D7565/D7565M, "Standard Test Method for Determining Tensile Properties of Fiber Reinforced Polymer Matrix Composites Used for Strengthening of Civil Structures," ASTM International, West Conshohocken, PA,, 2017.

23. West System, Epoxy Resin and Hardeners, https://www.westsystem.com.au/product-category/epoxy-resin-and-hardeners/, 2019. (last accessed Jan. 18, 2021)

24. AS 1012.9, "Methods of Testing Concrete-Determination of the Compressive Strength of Concrete Specimens," Standards Australia, 2014.

25. de Oliveira, D. S.; Raiz, V.; and Carrazedo, R., "Experimental Study on Normal-Strength, High-Strength and Ultrahigh-Strength Concrete Confined by Carbon and Glass FRP Laminates," *Journal of Composites for Construction*, ASCE, V. 23, No. 1, 2019, p. 04018072 doi: 10.1061/(ASCE)CC.1943-5614.0000912

26. ACI Committee 440, "Guide for the Design and Construction of Externally Bonded FRP Systems for Strengthening Concrete Structures (ACI 440.2R-08)," American Concrete Institute, Farmington Hills, MI, 2008.

27. Lam, L., and Teng, J. G., "Design-Oriented Stress-Strain Model for FRP-Confined Concrete," *Construction and Building Materials*, V. 17, No. 6-7, 2003, pp. 471-489. doi: 10.1016/S0950-0618(03)00045-X

28. Youssef, M. N.; Feng, M. Q.; and Mosallam, A. S., "Stress-Strain Model for Concrete Confined by FRP Composites," *Composites. Part B, Engineering*, V. 38, No. 5-6, 2007, pp. 614-628. doi: 10.1016/j.compositesb.2006.07.020

29. Berthet, J. F.; Ferrier, E.; and Hamelin, P., "Compressive Behavior of Concrete Externally Confined by Composite Jackets: Part B: Modeling," *Construction and Building Materials*, V. 20, No. 5, 2006, pp. 338-347. doi: 10.1016/j.conbuildmat.2005.01.029

30. Teng, J.; Huang, Y.; Lam, L.; and Ye, L., "Theoretical Model for Fiber-Reinforced Polymer-Confined Concrete," *Journal of Composites for Construction*, ASCE, V. 11, No. 2, 2007, pp. 201-210. doi: 10.1061/(ASCE)1090-0268(2007)11:2(201)

31. Jiang, T., and Teng, J., "Analysis-Oriented Stress-Strain Models for FRP-Confined Concrete," *Engineering Structures*, V. 29, No. 11, 2007, pp. 2968-2986. doi: 10.1016/j.engstruct.2007.01.010

32. Karbhari, V. M., and Gao, Y., "Composite Jacketed Concrete under Uniaxial Compression—Verification of Simple Design Equations," *Journal of Materials in Civil Engineering*, ASCE, V. 9, No. 4, 1997, pp. 185-193. doi: 10.1061/(ASCE)0899-1561(1997)9:4(185)

33. Samaan, M.; Mirmiran, A.; and Shahawy, M., "Model of Concrete Confined by Fiber Composites," *Journal of Structural Engineering*, ASCE, V. 124, No. 9, 1998, pp. 1025-1031. doi: 10.1061/(ASCE)0733-9445(1998)124:9(1025)

34. Cheng, H. L.; Sotelino, E. D.; and Chen, W. F., "Strength Estimation for FRP Wrapped Reinforced Concrete Columns," *Steel and Composite Structures*, V. 2, No. 1, 2002, pp. 1-20. doi: 10.12989/scs.2002.2.1.001

35. Wu, G.; Lü, Z. T.; and Wu, Z. S., "Strength and Ductility of Concrete Cylinders Confined with FRP Composites," *Construction and Building Materials*, V. 20, No. 3, 2006, pp. 134-148. doi: 10.1016/j.conbuildmat.2005.01.022

36. Tamuzs, V.; Tepfers, R.; and Sparnins, E., "Behavior of Concrete Cylinders Confined by Carbon Composite 2. Prediction of Strength," *Mechanics of Composite Materials*, V. 42, No. 2, 2006, pp. 109-118. doi: 10.1007/s11029-006-0022-7

37. Benzaid, R.; Mesbah, H.; and Chikh, N. E., "FRP-Confined Concrete Cylinders: Axial Compression Experiments and Strength Model," *Journal of Reinforced Plastics and Composites*, V. 29, No. 16, 2010, pp. 2469-2488. doi: 10.1177/0731684409355199

38. Wei, Y. Y., and Wu, Y. F., "Unified Stress-Strain Model of Concrete for FRP-Confined Columns," *Construction and Building Materials*, V. 26, No. 1, 2012, pp. 381-392. doi: 10.1016/j.conbuildmat.2011.06.037